Capillary Origami: Spontaneous Wrapping of a Droplet with an Elastic Sheet

Charlotte Py,[1,*] Paul Reverdy,[2] Lionel Doppler,[1] José Bico,[1] Benoît Roman,[1] and Charles N. Baroud[2]

[1]*Physique et Mécanique des Milieux Hétérogènes, ESPCI, Paris 6, Paris 7, UMR CNRS 7636, 75231 Paris cedex 5, France*

[2]*Laboratoire d'Hydrodynamique (LadHyX) and Département de Mécanique, École Polytechnique, UMR CNRS 7646, 91128 Palaiseau cedex, France*

(Received 27 November 2006; published 13 April 2007)

The interaction between elasticity and capillarity is used to produce three-dimensional structures through the wrapping of a liquid droplet by a planar sheet. The final encapsulated 3D shape is controlled by tailoring the initial geometry of the flat membrane. Balancing interfacial energy with elastic bending energy provides a critical length scale below which encapsulation cannot occur, which is verified experimentally. This length is found to depend on the thickness as $h^{3/2}$, a scaling favorable to miniaturization which suggests a new way of mass production of 3D micro- or nanoscale objects.

DOI: 10.1103/PhysRevLett.98.156103 PACS numbers: 68.08.−p, 46.32.+x, 81.16.Dn, 85.85.+j

Origami and haute couture design both rely on folding and assembling planar material to create elegant three-dimensional shapes whose variety and complexity are governed by the number, order, and orientation of folds. Folding is also a way to reduce the size of deployable structures in space industry (satellite pannels or sun sails [1]) as well as in nature (plant leaves folded in a bud [2]). In micro and nanofabrication, the folding of planar structures is a promising approach to build 3D objects, since most microfabrication technologies produce planar layers through surface etching [3].

While centimeter-sized objects may be folded using well disposed magnets [4], capillarity is a particularly relevant mechanism for microfabrication [5], as surface forces dominate over bulk forces at small scales. Indeed, the capillary attraction and stiction of wet slender structures may induce disastrous damage in micro and nanoscale devices [6–9], in addition to being involved in lung airway closure (neonatal respiratory distress syndrome) [10]. Capillary interactions have already been proposed as a way of assembling and orienting rigid objects in 2D at the surface of water [11] or in 3D by capillary bridges [12], while further studies have focused on the capillary induced deflection of elastic rods [13–15]. Recently, the multifolding of a flexible ribbon squeezed in a meniscus has also been described through an elegant experiment [16]. Here, we address the effect of capillary forces on a flat elastic membrane and we show how the spontaneous folding of a flexible sheet around a liquid droplet leads to a predetermined 3D shape.

Our experiments were conducted using polydimethylsiloxane (PDMS) membranes. The PDMS (Dow corning Sylgard 184, 10:1 polymer/curing agent mix) was spin coated at 24 °C on a glass microscope slide at rotation rates of 1000–2000 rpm. Once the PDMS was cured, this resulted in sheets with thickness in the range 80–40 μm.

During a typical experiment, a geometric shape is manually cut out from the PDMS layer and placed on a superhydrophobic surface. A drop of water, of volume 1–80 μL depending on membrane size, is deposited on the PDMS, while making sure that the water reaches all the corners of the flat sheet. The water is then allowed to evaporate at room temperature and a time lapse sequence of images is taken of the membrane-drop pair. As the water volume decreases from its initial value to complete evaporation, the surface tension of the liquid pulls the sheet around smaller volumes, thus increasingly curving it (Fig. 1). Sufficiently thin sheets eventually encapsulate the liquid with a shape that depends on the initial cut of the membrane.

In the simplest case, a drop is deposited on a square PDMS sheet, as shown in Fig. 1(a). This initially leads to the bending of the four corners towards the center of the

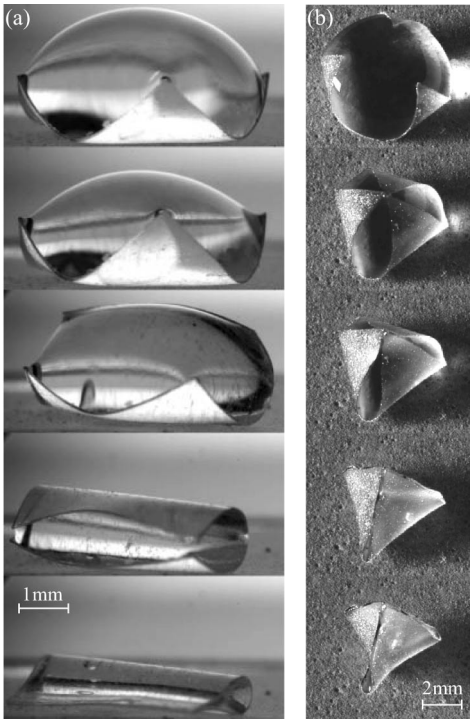

FIG. 1. Wrapping of a drop of water with (a) square and (b) triangular PDMS sheets. See movies Mov1 and Mov2 in Ref. [17].

sheet (mode-4). As the drop volume decreases further, this bending mode becomes unstable and the shape rapidly switches to a mode-2 state; in this state, the corners are attracted to each other two by two and the flat central region disappears, giving rise to a quasicylindrical shape [middle image in Fig. 1(a)]. As the drop volume decreases further, the approaching edges eventually touch and a water-filled tube is formed. Finally, the water evaporates completely and the tube enlarges into a loop whose ends merge into a flat contacting region, similar to the shape shown in Fig. 2(a).

A different situation occurs when a drop is deposited on a triangular sheet [image sequence in Fig. 1(b) and movie Mov2 in EPAPS [17]]. The corners fold towards the center as in the previous case, but this leads to a stable mode-3 folding. The three corners eventually join at the center and the sheet seals into a tetrahedral pyramid. At this stage, the curvature of the surface is concentrated around the edges of the pyramid, while the sides are almost flat [fourth image in Fig. 1(b)]. Further evaporation, which now occurs at a slower rate, finally leads to the buckling of the pyramid walls due to the negative internal pressure (final image).

For both of the above geometries, the scenario is different for membranes of smaller size or larger thickness. As the stiffness increases, the forces generated by surface tension become insufficient to achieve complete closure: after going through similar initial stages as for thin PDMS layers, a maximum bending of the sheet is produced after which it reopens again, never having produced an encapsulated drop (movie Mov3 in EPAPS [17]). The final state is therefore a planar sheet covered by a thin film of liquid which quickly evaporates.

The membrane deformations reduce the liquid-air area A and thus the surface energy γA (γ being the surface tension) at the cost of increasing the elastic energy. For a thin plate, the isometric bending energy density is defined locally as $B\kappa^2/2$, where κ is the curvature and $B = Eh^3/12(1-\nu^2)$ is the bending stiffness (E is the Young's modulus, ν the Poisson's ratio, and h the thickness) [18]. The ratio of these antagonistic terms dictates the typical radius of curvature L_{EC} generated by capillary forces for a given bending rigidity,

$$L_{\mathrm{EC}} = (B/\gamma)^{1/2}, \tag{1}$$

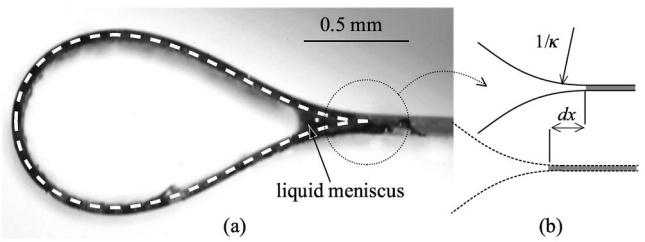

FIG. 2. (a) Experimental image of a loop of PDMS held by a meniscus of ethanol and comparison with the theoretical shape (dashed curve). (b) Virtual displacement dx of the meniscus position.

that we refer to as the *elasto-capillary length* [14]. Large deformations of the system are obtained when $L \gg L_{\mathrm{EC}}$. This scaling argument thus indicates that the critical size L_{crit} beyond which the sheet totally wraps the liquid droplet should be proportional to L_{EC}, the only characteristic length in the problem.

The elasto-capillary length can be directly measured through a calibration experiment rather than by estimating each parameter in Eq. (1) which would produce large errors. The experiment consists in depositing a drop of wetting liquid onto a very long strip of PDMS that folds over into a loop with a self-contacting tail. We consider the late stage, when only a small meniscus still holds the loop together [Fig. 2(a)].

This equilibrium state is 2D, so the following analysis is understood to be per unit depth. The cross section follows planar rod elasticity coupled with surface tension. We note $\theta(s)$ the angle made by the tangent to the rod $\mathbf{t}$ with respect to the horizontal, at curvilinear coordinate s. We also note $\mathbf{R}$ the constant vectorial tension of the beam, so that Euler's elastica equations for equilibrium may be expressed as [18]:

$$B\frac{d^2\theta}{ds^2}\mathbf{e_z} + \mathbf{t}\times\mathbf{R} = \mathbf{0}, \tag{2}$$

where $\mathbf{e_z}$ is the unit vector perpendicular to the plane of the section. The global shape of the loop is determined by elasticity, given the curvature at the contact point. In turn, this curvature is found from an equilibrium between surface tension and elasticity by considering a virtual displacement dx of the contact point for a loop of curvilinear length 2ℓ [see Fig. 2(b)]. The elastic energy, $E_{\mathrm{el}} = \int_{-\ell}^{\ell} B\kappa^2/2ds$, varies due to the change in the integral bounds, the integrand being stationary near elastic equilibrium. It may be written as $dE_{\mathrm{el}} = B\kappa_c^2 dx$, where κ_c is the curvature at the contact point. On the other hand, the variation of surface energy due to replacing a solid-gas interface (surface energy γ_{SG}) with a solid-liquid interface (γ_{SL}) is $2(\gamma_{\mathrm{SL}} - \gamma_{\mathrm{SG}})dx = 2\gamma\cos\alpha dx$, where α is the contact angle of the liquid on the surface (here we use ethanol which has a zero contact angle on the PDMS). Balancing the two energies yields the value of equilibrium curvature at the contact point: $\kappa_c = \sqrt{2}/L_{\mathrm{EC}}$.

The boundary value problem of Eq. (2) with the above boundary condition was solved numerically by enforcing the contact condition at the base of the loop, $\int_{-\ell}^{\ell}\sin(\theta)ds = 0$. L_{EC} was then measured by scaling the numerical solution to fit the experimental shape. An excellent agreement is obtained [dashed line superimposed on experimental picture in Fig. 2(a)]. In practice the width of the loop (theoretical value $0.89L_{\mathrm{EC}}$) is sufficient to determine L_{EC}.

The value of L_{EC} was measured for different membrane thicknesses and, for each thickness, the minimum length for encapsulation L_{crit} was determined for square and triangular membrane shapes (Fig. 3). The experimental

results are consistent with a linear relationship between L_{crit} and L_{EC} as expected from dimensional analysis [see discussion with Eq. (1)]. Based on this, a linear regression of the data leads to $L_{\mathrm{crit}} = 7.0 L_{\mathrm{EC}}$ for squares and $L_{\mathrm{crit}} = 11.9 L_{\mathrm{EC}}$ for triangles (Fig. 3).

Recovering the value of the critical length theoretically would require a full 3D description of the coupled thin plate and drop system. Here, we limit ourselves to a 2D model, which provides an understanding of the transition between the folding and reopening processes. Consider an elastic inextensible rod of length L bent by pressure and surface tension forces at its ends (inset in Fig. 4). Equation (2) still holds but the vectorial tension $\mathbf{R}$ is not constant anymore due to the pressure forces; it follows

$$\frac{d\mathbf{R}}{ds} + p\mathbf{n} = \mathbf{0}, \tag{3}$$

where $\mathbf{n}(\mathbf{s})$ is the unit vector normal to the rod. By neglecting gravity, the pressure p in the drop is uniform and the 2D shape of the liquid-air interface is a circular arc of radius $r = \gamma/p$.

Equations (2) and (3), with appropriate boundary conditions, are solved numerically and the distance δ between the rod tips is calculated as a function of drop section area S for different rod lengths L, as shown in Fig. 4. Two trivial flat states ($\delta/L = 1$) exist in all cases for an infinitely large drop (A and A') or when no liquid is present (B or B'). However, the evolution between these states is qualitatively different depending on L/L_{EC}.

For L/L_{EC} slightly below the critical value [Fig. 4(a)], these two states are connected by a continuous family of solutions from A to B: the drying of a large drop leads to transient limited bending but eventually to reopening as it is experimentally observed (Mov3 in EPAPS [17]). Closed states C do exist in a restricted domain of the phase space, as the stable segment of a solution loop, while the unstable part of this loop corresponds to a drop which has depinned from the edges D. This bistability is also observed in the experiments: while small sheets never close spontaneously, they can be forced into a closed state if the liquid is pulled out with a syringe.

Above the critical ratio L/L_{EC}, the drying of a large drop A' leads continuously to complete wrapping C' in agreement with experimental observations (Fig. 1 and Mov1 in EPAPS [17]). Another branch links the open state B' to unstable solutions D'. However, this branch is difficult to observe experimentally because it requires the spreading of a thin film of water on the flat membrane.

The 2D numerical simulation thus qualitatively reproduces the experimentally observed regimes and explains the closing-reopening transition. However, the crossing from diagrams (a) to (b) was found at $L_{\mathrm{crit}} = 3.54 L_{\mathrm{EC}}$, which is of the same order but below the value experimentally obtained for the square membranes. An improved model should include gravity and 3D effects.

Indeed, the drops considered in Fig. 3 are slightly flattened by gravity, since they are larger than the capillary length ($L_c = \sqrt{\gamma/\rho g}$, where ρ is the density of the liquid and g the acceleration of gravity). More importantly, the early stages are always 3D as seen in the initial folding of the corners of a square sheet. Only a full description of thin plate elasticity in 3D would account for the localization of the curvature around edges, which is reminiscent of the crumpling of thin sheets.

More generally, 3D wrapping of a droplet leads to a geometrical incompatibility described by Gauss's *theo-*

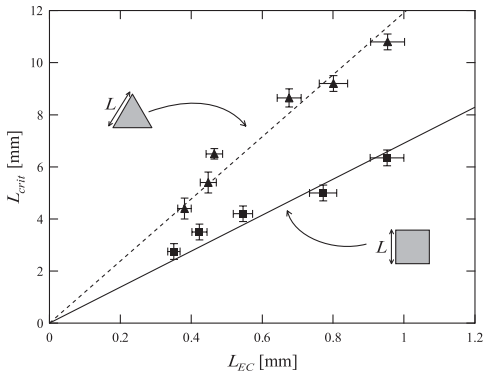

FIG. 3. Critical length for folding vs elasto-capillary length: black squares: square sheets, black triangles: triangular sheets, lines: linear regressions expected from dimensional analysis.

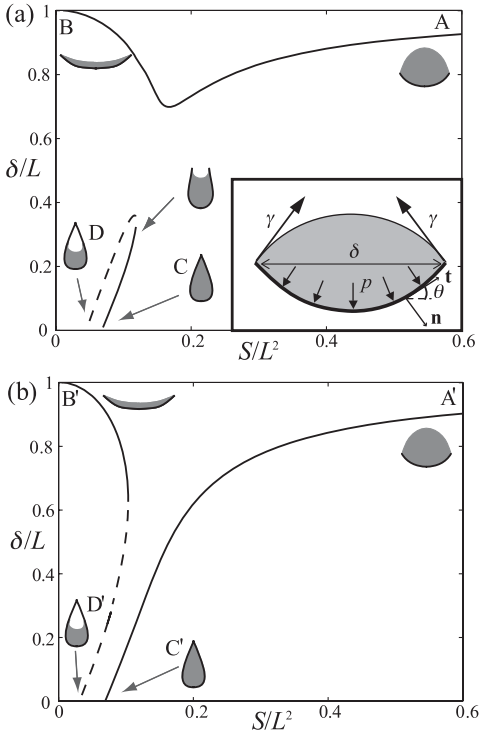

FIG. 4. Distance between the rod tips vs drop volume for different values of the rod length L: (a) $L = 3.4 L_{\mathrm{EC}}$ reopening of the rod as S decreases; (b) $L = 4 L_{\mathrm{EC}}$ complete wrapping of the rod around the drop. The inset shows a sketch of a 2D drop deposited on a flexible sheet.

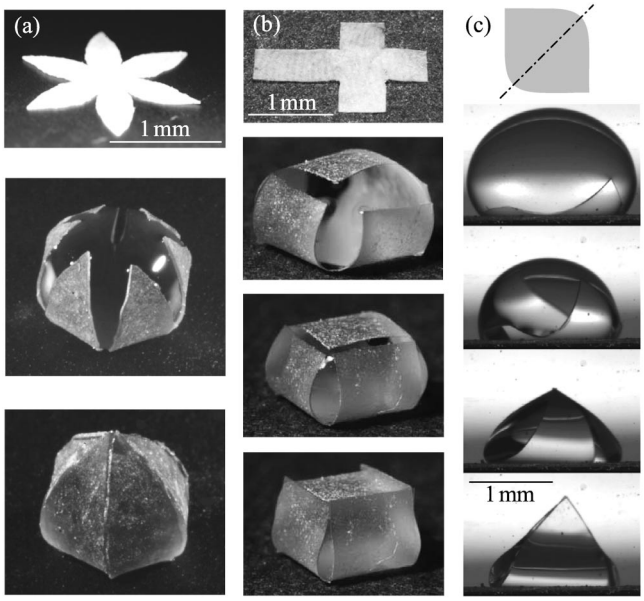

FIG. 5. Tuning of the initial flat shape to obtain (a) a spherical encapsulation, (b) a cubic encapsulation, or (c) a triangular mode-2 fold.

rema egregium. A classic example is that it is impossible to draw a planar map of the earth which conserves distances: the wrapping of a spherical object with a planar sheet must involve stretching as well as bending. For a thin membrane, the stretching energy scales as the thickness h and is therefore much more expensive than the bending energy which scales as h^3. The unavoidable stretching is therefore localized in singular regions, leading to crumpling singularities [19,20]. We expect that for $L \gg L_{EC}$, the number of singularities will increase since surface tension becomes dominant over elastic forces, leading to quasispherical crumpled encapsulated shapes.

Precise engineering of the final closed state may be obtained by tailoring the initial sheet geometry. In this way, it is possible to approximate a smooth sphere by starting with a flower shape, as shown in Fig. 5(a). Figure 5(b) shows how to form a cube by starting from a cross shape. As in the case of the pyramid, evaporation after encapsulation takes place at a reduced rate and may buckle the sphere or the cube due to the negative pressure thus generated. However, one may also freeze (or polymerize) the encapsulated liquid at any point in this process, therefore fixing the desired shape in place. Finally, small perturbations of the initial shape may also be used to yield different final states. In particular, rounding off two opposite corners of a square sheet leads to the membrane closing along its diagonal [Fig. 5(c)] rather than parallel to the sides. These experiments suggest that a wide variety of final shapes may be achieved through careful tuning of the initial flat shape.

In summary, three-dimensional submillimetric objects are produced from flat membranes through the interaction of elasticity and capillarity. The limitation on the minimal size for folding is determined by the elasto-capillary length [Eq. (1)] which scales as the sheet thickness $h^{3/2}$. This scaling is favorable to miniaturization since thinner membranes lead to much smaller critical lengths. This opens the way to mass production of microscale 3D structures based on standard microfabrication methods since a wide variety of objects can be fabricated by tailoring the initial planar sheet.

We are very grateful to Emmanuel de Langre for his insights and Anette (Peko) Hosoi for her cubic suggestions. This work was partly supported by the French ministry of research (ACI *Structures élastiques minces*) and the Société des Amis de l'ESPCI.

*Present address: Matière et Systèmes Complexes, Universitè Paris 7, UMR CNRS 7057, 75205 PARIS Cedex 13, France.

[1] D. D. Focatiis and S. Guest, Phil. Trans. R. Soc. A **360**, 227 (2002).
[2] H. Kobayashi, B. Kresling, and J. F. V. Vincent, Proc. R. Soc. B **265**, 147 (1998).
[3] M. Madou, *Fundamentals of Microfabrication: The Science of Miniaturization* (CRC Press, Boca Raton, FL, 2002), 2nd ed.
[4] M. Boncheva *et al.*, Proc. Natl. Acad. Sci. U.S.A. **102**, 3924 (2005).
[5] M. Boncheva, D. A. Bruzewicz, and G. M. Whitesides, Pure and Applied Chemistry **75**, 621 (2003).
[6] T. Tanaka, M. Morigami, and N. Atoda, Jpn. J. Appl. Phys. **32**, 6059 (1993).
[7] N. Chakrapani *et al.*, Proc. Natl. Acad. Sci. U.S.A. **101**, 4009 (2004).
[8] C. Mastrangelo and C. Hsu, J. Microelectromech. Syst. **2**, 33 (1993).
[9] O. Raccurt *et al.*, J. Micromech. Microeng. **14**, 1083 (2004).
[10] M. Heil and J. P. White, J. Fluid Mech. **462**, 79 (2002).
[11] N. Bowden *et al.*, J. Am. Chem. Soc. **121**, 5373 (1999).
[12] R. R. A. Syms *et al.*, J. Microelectromech. Syst. **12**, 387 (2003).
[13] A. E. Cohen and L. Mahadevan, Proc. Natl. Acad. Sci. U.S.A. **100**, 12 141 (2003).
[14] J. Bico, B. Roman, L. Moulin, and A. Boudaoud, Nature (London) **432**, 690 (2004).
[15] H. Y. Kim and L. Mahadevan, J. Fluid Mech. **548**, 141 (2006).
[16] K. G. Kornev *et al.*, Phys. Rev. Lett. **97**, 188303 (2006).
[17] See EPAPS Document No. E-PRLTAO-98-059716 for movie sequences from the experiments. For more information on EPAPS, see http://www.aip.org/pubservs/epaps.html.
[18] L. Landau and E. Lifshitz, *Theory of Elasticity* (Butterworth-Heinemann, Oxford, 1986), 3rd ed.
[19] A. Lobkovsky *et al.*, Science **270**, 1482 (1995).
[20] M. BenAmar and Y. Pomeau, Proc. R. Soc. A **453**, 729 (1997).